EUROPEAN ORGANIZATION FOR NUCLEAR RESEARCH
European Laboratory For Particle Physics

CERN-TIS-2002-005-RP-CF

ATTENUATION CURVES IN CONCRETE OF NEUTRONS FROM 100-400 MEV PER NUCLEON HE, C AND NE IONS

S. Agosteo[(1)], T. Nakamura[(2)] and **M. Silari[(3)]**

[(1)] Politecnico di Milano, Dipartimento di Energia Nucleare, Via Ponzio 34/3, 20133 Milano, Italy
[(2)] KEK, Department of Quantum Science and Energy Engineering, Cyclotron and Radioisotope Center, Tohoku University, Aoba, Aramaki, Aoba-ku, Sendai-shi 980-8578, Japan
[(3)] CERN, 1211 Geneva 23, Switzerland

Abstract

Data on transmission of neutrons in concrete generated by heavy ions of intermediate energies (of typically up to 1 GeV per nucleon) are of interest for shielding design of accelerators for use in both the research and in the medical field. The energy distributions of neutrons produced by ions of different species (from He to Xe) striking various targets at energies from 100 to 800 MeV per nucleon were recently measured by Kurosawa et al. in the angular range 0º – 90º. These spectra were used as input data for Monte Carlo simulations performed with the FLUKA code to determine source terms and attenuation lengths in ordinary concrete. Here calculations are presented for 100 MeV/u helium ions on a Cu target, 100 MeV/u carbon ions on C and Cu, 100 MeV/u neon ions on Cu and Pb, 400 MeV/u carbon ions on C, Al, Cu and Pb. The results include the contributions of all secondaries. Some of the resulting attenuation curves are best fitted by a double exponential function rather than the usual single one. The effect of various approximations introduced in the simulations is discussed.

To be presented at the SATIF-6 Workshop
10-12 April 2002, SLAC, Stanford, California, USA

CERN, 1211 Geneva 23, Switzerland
3 April 2002

Introduction

Experimental data on neutron emission from the interaction of heavy ion beams with matter are less abundant than data on neutron production from protons. In addition the various Monte Carlo codes applicable for radiation protection calculations, such as FLUKA [1,2], MCNPX [3] and MARS [4], do not treat secondary particle production from ions with masses larger than one atomic mass unit. Development work is under way to implement ion transport in FLUKA, but the new version of the code has not yet been released.

Thus there is a general lack of knowledge on shielding data, i.e. source terms and attenuation lengths, for neutron produced by heavy ions in all energy ranges. Recent experimental results obtained at CERN have shown that at very high energies the spectral fluence of the secondary neutrons outside a thick shield is similar for light (protons) and heavy (lead) ions of comparable energy per nucleon stopped in a thick target. It was also shown that the approach of considering a high-energy lead ion as an independent grouping of free protons is sufficiently accurate for the purpose of evaluating the ambient dose equivalent of secondary neutrons outside thick shielding [5].

Measurements of the neutron emission from comparatively thin, unshielded, targets have shown that the neutron spectral fluence has two peaks, i.e. an isotropic evaporation component centred at 3 MeV and a high-energy peak with a maximum around 100-150 MeV. A comparison with Monte Carlo simulations for protons and experimental results for lead ions has demonstrated that a reasonable prediction can be carried out by scaling the result of a Monte Carlo calculation for protons by the projectile mass number to a power law which slightly depends on the target [6,7].

Data on transmission in concrete of neutrons generated by heavy ions of intermediate energies (typically up to several hundreds of MeV per nucleon) are of interest for shielding design of accelerators for use in both the medical and the research field. As for the former, we shall here mention the various medical hadron accelerators being built for radiation therapy with ion beams. An example of the latter type of machines is the transformation of the former Low Energy Antiproton Ring (LEAR) at CERN into a Low Energy Ion Ring (LEIR) for the LHC injector chain.

Systematic measurements of yield and energy distribution in the angular range 0º-90º of neutrons produced by the interaction with various targets of ion beams from carbon to xenon with energy of up to 800 MeV per nucleon were recently published by Kurosawa et al. [8-10]. These spectra were used as input data for Monte Carlo simulations performed with the FLUKA code to determine source terms and attenuation lengths in ordinary concrete. Calculations are here presented for 100 MeV/u helium ions on a Cu target, 100 MeV/u carbon ions on C and Cu, 100 MeV/u neon ions on Cu and Pb, 400 MeV/u carbon ions on C, Al, Cu and Pb. The results include the contributions of all secondaries. The effect of various approximations introduced in the simulations is discussed. The way of employing the present results in shielding estimates using the Moyer model is addressed.

Neutron sources

Figure 1 shows the thick-target neutron yield (forward 2π) [8-10] as a function of the projectile mass number for the ion-target combinations considered in the present work. It should be noted that, for 400 MeV/u carbon ions, the neutron yield decreases with target mass number up to copper. The lead target yield is higher than that of copper and aluminium and is very close to that from a carbon target. A decreasing trend of the yield with target atomic number (for C and Cu) can also be observed for carbon ions at 100 MeV/u.

It should be mentioned that the energy distribution of secondary neutrons exceeds the energy per nucleon of the projectile, mainly at forward angles [8-10]. The maximum energy of the neutron spectra at forward angles is about 250 MeV and 1 GeV for 100 MeV/u and 400MeV/u ions, respectively. Therefore the corresponding attenuation lengths in concrete are expected to be larger than those of proton beams of the same energy.

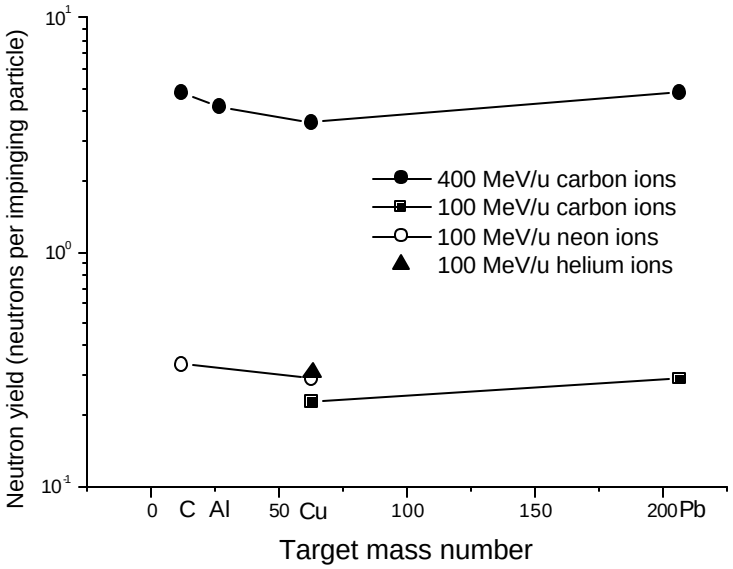

Figure 1. Thick-target neutron yield (forward 2π) [8-10] as a function of the projectile mass number for the ion energies considered in this work.

Monte Carlo calculations

The following simulation geometry was used for calculating the source terms and the attenuation lengths. A point neutron source was placed at the centre of a spherical shell, 6 m thick, made up of concrete TSF-5.5 [11], with inner radius large enough (90 m) to make effects related to curvature negligible. Effects due to neutron scattering are also negligible, since the fluence of neutrons diffusing inside the concrete shell is inversely dependent on its inner surface area [12]. The fluence of outward-directed particles was scored in boundary crossings placed at various depths inside the concrete shell. The latter was also subdivided into polar sectors to account for the angular distribution of the fluence. At projectile energies of 400 MeV/u, where the energy distribution of the secondary neutrons exceeds the threshold energy for pion production (about 280 MeV [13]), the fluence of pions generated in concrete was scored in addition to that of neutrons, photons (from neutron absorption and residual nucleus de-excitation) and secondary protons. The ambient dose equivalent was estimated with the conversion coefficients of refs. [14-15]. Geometry splitting and Russian roulette were used as variance reduction techniques for neutron transport inside the concrete shield.

As mentioned above, fluence scoring in each boundary crossing inside the concrete shells accounted only for outward-directed particles. This should minimize the effect of reflection (especially for neutrons) from the outer concrete shells, which leads to overestimate the fluence and consequently H*(10). However, reflection is not eliminated completely because, as a second order effect, neutrons can be backscattered more than once inside the shield. Each time a multi-reflected neutron crosses a

boundary outwards, it is counted in this one-way fluence scoring. Moreover, since neutrons are slowed down in scattering events, the prompt gamma-ray component from low-energy neutrons may also be overestimated. The exact evaluation would have required a set of different simulations, each one with the correct shielding thickness, and a much longer computing time. The effect of this approximation was investigated with separate simulations considering shells with different thickness, for the case of 400 MeV/u carbon ions on copper [16]. Data were fitted with the classical two-parameter formula (single-exponential function), given by expression (1) in the following Section. As expected, the source terms resulted to be slightly lower (in the range 2%-13%, excluding the angular bins 30°-40° and 80°-90°) than those calculated with fictitious shells. The difference in the attenuation lengths was found to be comparatively small (a few percent at maximum). It can therefore be concluded that, at least for 400 MeV/u carbon ions on copper, the data obtained with the fictitious shell model are sufficiently correct and representative of the real situation, if the overall non-statistical uncertainties (i.e. cross sections, nuclear models, concrete composition, etc.) are also taken into account.

Results

The attenuation curves in concrete at 0°-10° and 80°-90° for 100 MeV/u neon and 400 MeV/u carbon ions on copper are shown as an example in Figures 2 and 3, respectively. It has been shown previously [16] that neutrons are responsible for most of the dose equivalent, but also that the contribution of secondary protons cannot be completely neglected.

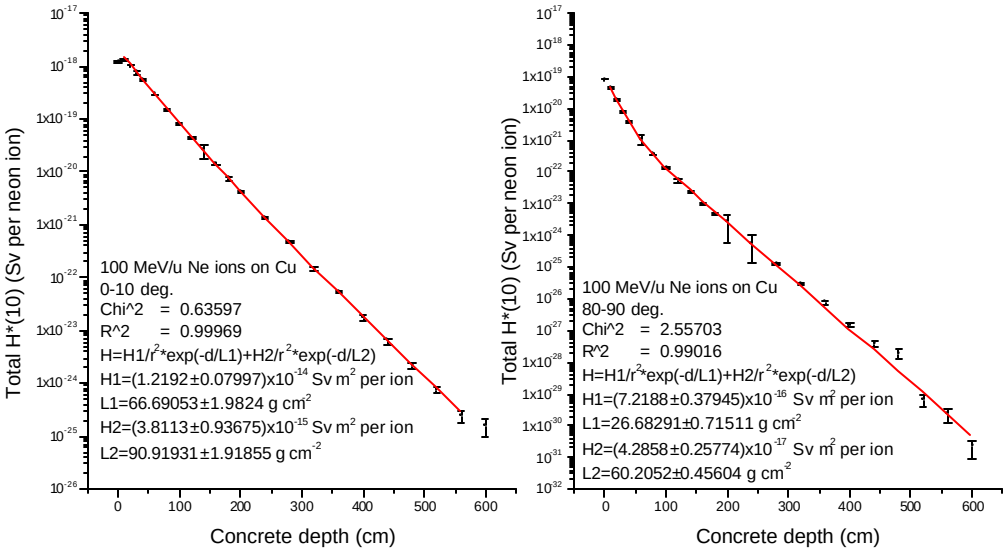

Figure 2. Attenuation curves in concrete at 0º-10º and 80º-90º for 100 MeV/u neon ions on copper.

The data at forward angles (up to 50°) for 400 MeV/u projectiles are characterised by a build-up behaviour. No build-up is observed at larger angles and small depths (up to about 60 cm), where the curves decrease with a slope steeper than at equilibrium. This double-exponential trend characterises also the attenuation curves for 100 MeV/u ions at all angles. This effect may be explained by observing how the neutron spectra vary with depth in concrete. The following discussion refers to the

spectral fluences at 80°-90° in concrete shown in Figure 4 for 400 MeV/u carbon ions on copper, but holds generally for the other ion-target combinations considered in this work. At 20 cm depth a broad peak is present with a maximum at around 50 MeV. At larger depths, up to about 100 cm, the peak tends to get narrower and to be displaced towards higher energies (about 100 MeV). This trend is quite smooth below 100 cm and yields to a "quasi-equilibrium" situation. The spectral fluence then reaches its equilibrium. In other words, the lower energy components of the spectrum are attenuated mostly up to about 100 cm concrete depth with a short attenuation length, giving rise to a harder and more penetrating spectral distribution (even if less intense), which is characterised by a larger attenuation length.

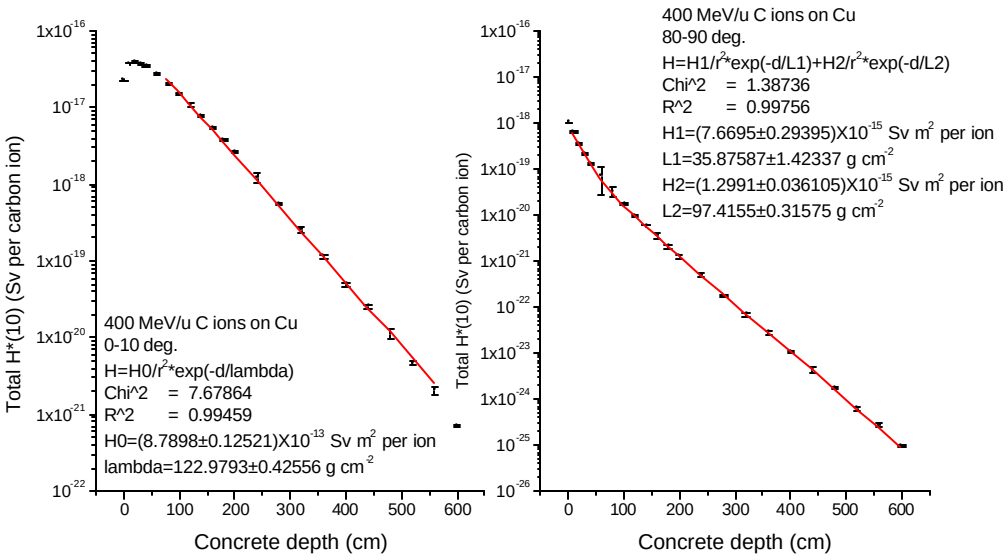

Figure 3. Attenuation curves in concrete at 0°-10° and 80°-90° for 400 MeV/u carbon ions on copper.

The attenuation curves of 400 MeV/u carbon ions on carbon, aluminium, copper and lead were fitted with the classical two-parameter formula for angles up to 50° (40° for 400 MeV/u C ions on lead):

$$H(E_p, q, d/l) = \frac{H_0(E_p, q)}{r^2} \exp\left[-\frac{d}{l_q \; g(a)}\right] \qquad (1)$$

where H is the ambient dose equivalent beyond the shield, E_p is the energy per nucleon of the primary particle (neutrons in the present case), r is the distance between the radiation source and the scoring position, θ is the angle between the direction $\vec{r}$ and the beam axis, H_0 is the neutron source term, d is the shield thickness, λ_θ is the attenuation length and α is the angle between the direction $\vec{r}$ and the normal to the shield surface. The function $g(\alpha) = 1$ for the spherical geometry used in the present simulations and $g(\alpha) = \cos\alpha$ in all other cases.

A double-exponential function was used for fitting the attenuation curves of 400 MeV/u carbon ions on carbon, aluminium, copper and lead for angles above 50° and those of 100 MeV/u helium, carbon and neon ions:

$$H(E_p,q,d/l)=\frac{H_1(E_p,q)}{r^2}\exp\left[-\frac{d}{l_{1,q}\ g(a)}\right]+\frac{H_2(E_p,q)}{r^2}\exp\left[-\frac{d}{l_{2q}\ g(a)}\right] \qquad (2)$$

where (H_1, $\lambda_{1,\theta}$) and (H_2, $\lambda_{2,\theta}$) are the source terms and the attenuation lengths of the low-depth and high-depth exponential functions, respectively. The second term of expression (2) describes the attenuation above 60-100 cm and obviously cannot be applied at lower depths, because it would lead to an underestimate of the ambient dose equivalent. In practice, expression (2) includes expression (1) by setting $H_0 = H_2$, $\lambda_\theta = \lambda_{2,\theta}$ and setting the first term to zero (i.e., $H_1 = \lambda_{1,\theta} = 0$).

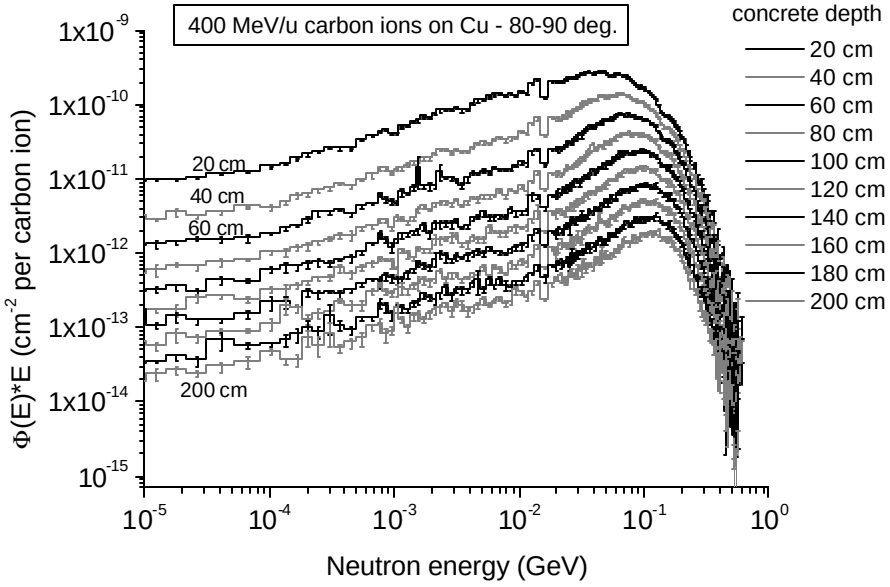

Figure 4. Neutron spectral fluences at various depths in concrete, at 80°-90°, for 400 MeV/u carbon ions on copper.

The resulting source terms and the attenuation lengths are listed in Tables 1-9, for 100 MeV/u helium ions on a Cu target, 100 MeV/u C on C and Cu targets, 100 MeV/u Ne ions on Cu and Pb targets and 400 MeV/u C ions on C, Al, Cu and Pb targets.

Table 1. Source terms and attenuation lengths in concrete for neutrons generated by 100 MeV/u helium ions on Cu. The data were fitted using expression (2).

Angular bin	H_1 (Sv m^2 per ion)	λ_1 (g cm^{-2})	H_2 (Sv m^2 per ion)	λ_2 (g cm^{-2})
0-10°	(6.43±0.76)x10^{-15}	64.17±4.58	(7.11±0.92)x10^{-15}	94.12±1.22
10-20°	(4.57±0.17)x10^{-15}	51.11±2.46	(3.43±0.19)x10^{-15}	92.34±0.67
20-30°	(3.88±0.15)x10^{-15}	47.78±1.69	(1.12±0.09)x10^{-15}	90.59±0.94
30-40°	(3.29±0.18)x10^{-15}	35.97±1.23	(6.46±0.37)x10^{-16}	82.55±0.74
40-50°	(2.23±0.15)x10^{-15}	33.62±1.16	(2.64±0.16)x10^{-16}	81.61±0.64
50-60°	(1.64±0.12)x10^{-15}	29.43±0.95	(9.94±0.39)x10^{-17}	77.22±0.54
60-70°	(1.34±0.08)x10^{-15}	27.02±0.74	(4.91±0.34)x10^{-17}	66.56±0.77
70-80°	(1.27±0.05)x10^{-15}	24.82±0.43	(5.40±0.62)x10^{-17}	50.57±0.82
80-90°	(1.33±0.08)x10^{-15}	20.98±0.52	(7.40±0.80)x10^{-17}	42.30±0.63

Table 2. Source terms and attenuation lengths in concrete for neutrons generated by 100 MeV/u carbon ions on C. The data were fitted using expression (2).

Angular bin	H_1 (Sv m^2 per ion)	λ_1 (g cm^{-2})	H_2 (Sv m^2 per ion)	λ_2 (g cm^{-2})
0-10°	$(2.84\pm0.10)\times10^{-14}$	59.10±1.40	$(9.06\pm1.24)\times10^{-15}$	86.91±1.07
10-20°	$(1.31\pm0.04)\times10^{-14}$	54.08±1.97	$(4.08\pm0.46)\times10^{-15}$	88.31±1.03
20-30°	$(5.40\pm0.39)\times10^{-15}$	47.99±1.87	$(1.77\pm0.10)\times10^{-15}$	87.59±0.64
30-40°	$(2.53\pm0.16)\times10^{-15}$	46.37±1.82	$(6.83\pm0.43)\times10^{-16}$	88.14±0.68
40-50°	$(1.91\pm0.05)\times10^{-15}$	40.92±0.95	$(3.87\pm0.15)\times10^{-16}$	87.62±0.54
50-60°	$(1.10\pm0.06)\times10^{-15}$	37.64±1.37	$(2.14\pm0.09)\times10^{-16}$	85.64±0.57
60-70°	$(8.40\pm0.40)\times10^{-16}$	33.13±0.92	$(8.97\pm0.43)\times10^{-17}$	82.52±0.69
70-80°	$(5.70\pm0.40)\times10^{-16}$	32.70±1.24	$(3.89\pm0.30)\times10^{-17}$	73.23±0.73
80-90°	$(3.97\pm0.14)\times10^{-16}$	31.32±0.42	$(1.07\pm0.07)\times10^{-17}$	73.47±0.67

Table 3. Source terms and attenuation lengths in concrete for neutrons generated by 100 MeV/u carbon ions on Cu. The data were fitted using expression (2).

Angular bin	H_1 (Sv m^2 per ion)	λ_1 (g cm^{-2})	H_2 (Sv m^2 per ion)	λ_2 (g cm^{-2})
0-10°	$(1.65\pm0.64)\times10^{-14}$	58.72±1.80	$(4.44\pm0.80)\times10^{-15}$	89.32±1.66
10-20°	$(8.77\pm0.20)\times10^{-15}$	49.23±0.93	$(2.34\pm0.12)\times10^{-15}$	89.70±0.60
20-30°	$(4.74\pm0.17)\times10^{-15}$	42.28±1.23	$(1.22\pm0.06)\times10^{-15}$	87.06±0.57
30-40°	$(2.75\pm0.12)\times10^{-15}$	37.73±1.47	$(5.75\pm0.37)\times10^{-16}$	81.11±0.70
40-50°	$(1.91\pm0.05)\times10^{-15}$	40.92±0.95	$(3.87\pm0.15)\times10^{-16}$	87.62±0.54
50-60°	$(1.70\pm0.15)\times10^{-15}$	39.34±1.58	$(2.15\pm0.19)\times10^{-16}$	76.87±0.87
60-70°	$(1.27\pm0.13)\times10^{-15}$	31.47±1.50	$(1.88\pm0.12)\times10^{-16}$	64.74±0.61
70-80°	$(6.56\pm0.83)\times10^{-16}$	30.91±1.31	$(5.51\pm0.32)\times10^{-17}$	70.40±0.57
80-90°	$(4.44\pm0.25)\times10^{-16}$	33.27±0.60	$(2.16\pm0.11)\times10^{-17}$	82.88±0.50

Table 4. Source terms and attenuation lengths in concrete for neutrons generated by 100 MeV/u neon ions on Cu. The data were fitted using expression (2).

Angular bin	H_1 (Sv m^2 per ion)	λ_1 (g cm^{-2})	H_2 (Sv m^2 per ion)	λ_2 (g cm^{-2})
0-10°	$(1.22\pm0.08)\times10^{-14}$	66.69±1.98	$(3.81\pm0.94)\times10^{-15}$	90.92±1.92
10-20°	$(6.61\pm0.23)\times10^{-15}$	62.68±1.42	$(1.75\pm0.27)\times10^{-15}$	94.15±1.43
20-30°	$(3.64\pm0.06)\times10^{-15}$	47.27±0.94	$(1.44\pm0.07)\times10^{-15}$	93.38±0.63
30-40°	$(2.72\pm0.45)\times10^{-15}$	39.06±0.81	$(8.13\pm0.21)\times10^{-16}$	94.28±0.51
40-50°	$(2.04\pm0.04)\times10^{-15}$	38.43±0.65	$(3.14\pm0.13)\times10^{-16}$	92.73±0.70
50-60°	$(1.62\pm0.22)\times10^{-15}$	30.75±0.50	$(1.54\pm0.06)\times10^{-16}$	85.70±0.58
60-70°	$(1.12\pm0.05)\times10^{-15}$	30.65±0.65	$(5.95\pm0.36)\times10^{-17}$	79.97±0.76
70-80°	$(9.42\pm0.40)\times10^{-16}$	27.95±0.56	$(5.48\pm0.33)\times10^{-17}$	67.15±0.61
80-90°	$(7.22\pm0.38)\times10^{-16}$	26.68±0.71	$(4.29\pm0.26)\times10^{-17}$	60.20±0.46

Table 5. Source terms and attenuation lengths in concrete for neutrons generated by 100 MeV/u neon ions on Pb. The data were fitted using expression (2).

Angular bin	H_1 (Sv m^2 per ion)	λ_1 (g cm^{-2})	H_2 (Sv m^2 per ion)	λ_2 (g cm^{-2})
0-10°	$(7.68\pm0.80)\times10^{-15}$	58.15±4.16	$(5.47\pm1.09)\times10^{-15}$	81.31±1.35
10-20°	$(4.63\pm0.22)\times10^{-15}$	54.60±2.89	$(2.34\pm0.30)\times10^{-15}$	85.69±1.14
20-30°	$(3.52\pm0.06)\times10^{-15}$	46.27±1.24	$(1.03\pm0.06)\times10^{-15}$	87.68±0.69
30-40°	$(2.74\pm0.17)\times10^{-15}$	36.31±1.68	$(6.70\pm0.35)\times10^{-16}$	83.54±0.62
40-50°	$(2.01\pm0.11)\times10^{-15}$	37.50±1.26	$(2.88\pm0.17)\times10^{-16}$	87.32±0.72
50-60°	$(1.65\pm0.07)\times10^{-15}$	32.24±0.73	$(1.76\pm0.01)\times10^{-16}$	82.24±0.60
60-70°	$(1.06\pm0.07)\times10^{-15}$	33.51±1.07	$(7.35\pm0.48)\times10^{-17}$	81.99±0.87
70-80°	$(7.03\pm0.40)\times10^{-16}$	37.63±0.78	$(3.00\pm0.29)\times10^{-17}$	77.52±0.95
80-90°	$(1.03\pm0.04)\times10^{-15}$	28.11±0.45	$(2.26\pm0.14)\times10^{-17}$	74.47±0.59

Table 6. Source terms and attenuation lengths in concrete for neutrons generated by 400 MeV/u carbon ions on C. The data were fitted using expression (2).

Angular bin	H_1 (Sv m^2 per ion)	λ_1 (g cm^{-2})	H_2 (Sv m^2 per ion)	λ_2 (g cm^{-2})
0-10°			$(1.93\pm0.02)\times10^{-12}$	120.98±0.21
10-20°			$(4.37\pm0.02)\times10^{-13}$	120.21±0.14
20-30°			$(1.50\pm0.01)\times10^{-13}$	122.15±0.20
30-40°			$(5.75\pm0.03)\times10^{-14}$	122.18±0.21
40-50°			$(2.28\pm0.02)\times10^{-14}$	117.03±0.21
50-60°	$(1.03\pm0.05)\times10^{-14}$	49.28±2.27	$(7.53\pm0.15)\times10^{-15}$	111.74±0.34
60-70°	$(8.98\pm0.33)\times10^{-15}$	50.07±1.59	$(3.19\pm0.14)\times10^{-15}$	103.86±0.65
70-80°	$(7.62\pm0.28)\times10^{-15}$	48.43±1.40	$(1.49\pm0.07)\times10^{-15}$	102.23±0.64
80-90°	$(6.11\pm0.33)\times10^{-15}$	39.88±1.07	$(9.54\pm0.26)\times10^{-16}$	95.87±0.36

Table 7. Source terms and attenuation lengths in concrete for neutrons generated by 400 MeV/u carbon ions on Al. The data were fitted using expression (2).

Angular bin	H_1 (Sv m^2 per ion)	λ_1 (g cm^{-2})	H_2 (Sv m^2 per ion)	λ_2 (g cm^{-2})
0-10°			$(1.38\pm0.01)\times10^{-12}$	117.92±0.18
10-20°			$(2.69\pm0.01)\times10^{-13}$	121.15±0.19
20-30°			$(1.14\pm0.01)\times10^{-13}$	119.69±0.20
30-40°			$(5.61\pm0.05)\times10^{-14}$	117.67±0.21
40-50°			$(2.03\pm0.01)\times10^{-14}$	114.30±0.22
50-60°	$(9.60\pm0.95)\times10^{-15}$	45.22±3.02	$(7.51\pm0.18)\times10^{-15}$	109.87±0.32
60-70°	$(8.14\pm0.38)\times10^{-15}$	53.92±2.75	$(2.85\pm0.21)\times10^{-15}$	106.68±0.98
70-80°	$(7.33\pm0.43)\times10^{-15}$	48.25±1.73	$(1.73\pm0.06)\times10^{-15}$	102.60±0.45
80-90°	$(5.96\pm0.22)\times10^{-15}$	46.32±1.30	$(9.05\pm0.47)\times10^{-16}$	99.41±0.50

Table 8. Source terms and attenuation lengths in concrete for neutrons generated by 400 MeV/u carbon ions on Cu. The data were fitted using expression (2).

Angular bin	H_1 (Sv m^2 per ion)	λ_1 (g cm^{-2})	H_2 (Sv m^2 per ion)	λ_2 (g cm^{-2})
0-10°			$(8.79\pm0.12)\times10^{-13}$	122.98±0.43
10-20°			$(2.13\pm0.01)\times10^{-13}$	121.62±0.14
20-30°			$(8.75\pm0.06)\times10^{-14}$	121.21±0.19
30-40°			$(3.58\pm0.01)\times10^{-14}$	122.47±0.15
40-50°			$(1.93\pm0.02)\times10^{-14}$	119.16±0.19
50-60°	$(1.11\pm0.13)\times10^{-14}$	30.93±2.28	$(8.10\pm0.09)\times10^{-15}$	120.91±0.24
60-70°	$(7.83\pm0.56)\times10^{-15}$	47.47±2.63	$(2.91\pm0.10)\times10^{-15}$	116.03±2.53
70-80°	$(6.78\pm0.51)\times10^{-15}$	45.61±2.05	$(1.88\pm0.06)\times10^{-15}$	102.46±0.39
80-90°	$(7.67\pm0.29)\times10^{-15}$	35.88±1.42	$(1.30\pm0.04)\times10^{-15}$	97.42±0.32

Table 9. Source terms and attenuation lengths in concrete for neutrons generated by 400 MeV/u carbon ions on Pb. The data were fitted using expression (2).

Angular bin	H_1 (Sv m^2 per ion)	λ_1 (g cm^{-2})	H_2 (Sv m^2 per ion)	λ_2 (g cm^{-2})
0-10°			$(7.17\pm0.10)\times10^{-13}$	118.11±0.25
10-20°			$(1.68\pm0.01)\times10^{-13}$	121.67±0.22
20-30°			$(7.05\pm0.06)\times10^{-14}$	121.44±0.23
30-40°			$(3.05\pm0.02)\times10^{-14}$	115.65±0.25
40-50°	$(2.12\pm0.24)\times10^{-14}$	30.99±2.40	$(1.29\pm0.02)\times10^{-14}$	108.64±0.32
50-60°	$(1.50\pm0.13)\times10^{-14}$	37.18±2.03	$(6.17\pm0.14)\times10^{-15}$	100.52±0.40
60-70°	$(1.67\pm0.10)\times10^{-14}$	33.88±1.26	$(3.67\pm0.09)\times10^{-15}$	95.55±0.37
70-80°	$(1.01\pm0.10)\times10^{-14}$	41.37±2.05	$(2.26\pm0.08)\times10^{-15}$	98.40±0.35
80-90°	$(1.08\pm0.06)\times10^{-14}$	37.67±1.38	$(1.03\pm0.47)\times10^{-15}$	99.84±0.34

The source terms and attenuation lengths tend to decrease with increasing angle, according to the yield and the energy distribution of secondary neutrons [8-10]. In the interval 0°-30° the source terms for 400 MeV/u carbon ions on carbon are higher (up to a factor 1.6) than those for aluminium. At forward angles the source terms for C ions on C and Al are higher than those for copper and lead. This difference tends to vanish at larger angles, where the attenuation lengths are also comparable. This is in agreement with the high-energy components (above about 20 MeV) of the neutron yield for C ions on C, Al, Cu and Pb targets [8], which do not differ too much at large angles. The source terms and the attenuation lengths for 400 MeV/u carbon ions on carbon and copper targets are also given in ref. [16], where a single-exponential function was used for data fitting. The resulting parameters at large angles agree satisfactorily with the H_2 and λ_2 calculated in the present work for the same ion-target combinations.

Conclusions

The approach of considering an ion of mass A equivalent to a bunch of A protons is most likely not a good approximation in the energy range discussed here. This is correct at ultra-relativistic energies, i.e. hundreds of GeV/u, as has been experimentally verified in recent years [5-7,17], but here it may lead to underestimates rather than overestimates. A quick comparison of shielding data for 100 MeV/u Ne ions on a copper target (resulting from the present Monte Carlo calculations) with those for 100 MeV protons on an iron target [18], seems to indicate that assuming the ion as a bunch of free protons would underestimate the shielding requirement by a factor which becomes increasingly larger with increasing shielding thickness. This is most likely because secondary neutrons from ion beams have a spectrum that extends to a maximum energy which is almost twice the projectile energy per nucleon, as has been shown above. This penetrating component would dominate the radiation dose past a thick shield. This trend will be studied in more detail in the continuation of this work.

References

[1] A. Fassò, A. Ferrari, P.R. Sala, *Electron-photon transport in FLUKA: status*, Proceedings of the Monte Carlo 2000 Conference, Lisbon, 23-26 October 2000, A. Kling, F. Barao, M. Nakagawa, L. Tavora, P. Vaz eds., Springer-Verlag Berlin, pp. 159-164 (2001).

[2] A. Fassò, A. Ferrari, J. Ranft, P.R. Sala, *FLUKA: Status and prospective for hadronic applications*, Proceedings of the Monte Carlo 2000 Conference, Lisbon, 23-26 October 2000, A. Kling, F. Barao, M. Nakagawa, L. Tavora, P. Vaz eds., Springer-Verlag Berlin, pp. 955-960 (2001).

[3] R.E. Prael and H. Lichtenstein, *User guide to LCS: The LAHET Code System*, LA-UR-89-3014, Los Alamos National Laboratory, Los Alamos, New Mexico (1989).

[4] N.V. Mokhov, S.I. Striganov, A. Van Ginneken, S.G. Mashnik, A.J. Sierk and J. Ranft, *MARS code developments*, Proceedings of the Fourth Workshop on Simulating Accelerator Radiation Environments (SARE4), Knoxville (TN, USA), 14-16 September 1998, Ed. T. Gabriel, ORNL (1998) 87-99.

[5] S. Agosteo, C. Birattari, A. Foglio Para, M. Silari and L. Ulrici, *Neutron measurements around a beam dump bombarded by high energy protons and lead ions*, Nuclear Instruments and Methods A 459, 58-65, 2001.

[6] S. Agosteo, C. Birattari, A. Foglio Para, A. Mitaroff, M. Silari and L. Ulrici, *90° neutron emission from high energy protons and lead ions on a thin lead target*, Nuclear Instruments and Methods A 476, 63-68, 2002.

[7] S. Agosteo, C. Birattari, A. Foglio Para, L. Gini, A. Mitaroff, M. Silari and L. Ulrici, *Neutron production from 158 GeV/c per nucleon lead ions on thin copper and lead targets in the angular range 30º – 135º*, submitted for publication in Nuclear Instruments and Methods B.

[8] T. Kurosawa, N. Nakao, T. Nakamura, Y. Uwamino, T. Shibata, N. Nakanishi, A. Fukumura and K. Murakami, *Measurements of secondary neutrons produced from thick targets bombarded by high-energy helium and carbon ions*, Nuclear Science and Engineering 132, 30-57, 1999.

[9] T. Kurosawa, N. Nakao, T. Nakamura, Y. Uwamino, T. Shibata, A. Fukumura and K. Murakami, *Measurements of secondary neutrons produced from thick targets bombarded by high energy neon ions*, Journal of nuclear science and technology, 36, 41-53, 1999.

[10] T. Kurosawa, N. Nakao, T. Nakamura, H. Iwase, H. Sato, Y. Uwamino and A. Fukumura, *Neutron yields from thick C, Al, Cu and Pb targets bombarded by 400 MeV/nucleon Ar, Fe, Xe and 800 MeV/nucleon Si ions*, Physical Review C 62, Third series, No. 4, 2000.

[11] National Council of Radiation Protection, *Radiation protection design guidelines for 0.1-100 MeV Particle Accelerators Facilities*, NCRP Report 51, 1977.

[12] R.C. McCall, T.M. Jenkins, R.A. Shore, *Transport of accelerator produced neutrons in a concrete room*, IEEE Trans. Nucl. Sci. NS-26, 1593-1602, 1979.

[13] A. Ferrari, P.R. Sala, *The physics of high energy reactions*, Proceedings of the Workshop on Nuclear Reaction Data and Nuclear Reactor Physics, Design and Safety, International Centre for Theoretical Physics, Miramare-Trieste (Italy), 15 April-17 May 1996. Edited by A. Gandini, and G. Reffo, Vol.2, World Scientific, 424-532, 1998.

[14] A. Ferrari and M. Pelliccioni, *Fluence to dose equivalent conversion data and effective quality factors for high energy neutrons*, Radiation Protection Dosimetry 76, 215-224, 1998.

[15] M. Pelliccioni, *Overview of fluence-to-effective dose and fluence-to-ambient dose equivalent conversion coefficients for high energy radiation calculated using the FLUKA code*, Radiation Protection Dosimetry 88, 279-297, 2000.

[16] S. Agosteo, *Radiation protection at medical accelerators*, Radiation Protection Dosimetry 96, 393-406, 2001.

[17] S. Agosteo, C. Birattari, A. Foglio Para, E. Nava, M. Silari and L. Ulrici, *Neutron measurements in the stray field produced by 158 GeV/c lead ion beams*, Health Physics 75, 619-629, 1998.

[18] S. Agosteo, A. Fassò, A. Ferrari, P.R. Sala, M. Silari and P. Tabarelli de Fatis, *Double differential distributions and attenuation in concrete for neutrons produced by 100-400 MeV protons on iron and tissue targets*, Nuclear Instruments and Methods B 114, 70-80, 1996.